INSTITUTE OF PHYSICS PUBLISHING NANOTECHNOLOGY
Nanotechnology **16** (2005) 2402–2406 doi:10.1088/0957-4484/16/10/068

Surface crystallization effects on the optical and electric properties of CdS nanorods

Anlian Pan[1,2], Xiao Lin[2], Ruibin Liu[1,2], Chaorong Li[2], Xiaobo He[2], Hongjun Gao[2] and Bingsuo Zou[1,2,3]

[1] Micro–Nano Technologies Research Center, Hunan University, Changsha 410082, People's Republic of China
[2] Institute of Physics, Chinese Academy of Sciences, Beijing 100080, People's Republic of China

E-mail: zoubs@aphy.iphy.ac.cn

Received 6 July 2005, in final form 11 August 2005
Published 2 September 2005
Online at stacks.iop.org/Nano/16/2402

Abstract
We synthesized CdS nanorods through a conventional solvothermal method and studied their photoluminescence and electric transport properties before and after annealing. High-resolution transmission electron microscopy indicated that the surface layer of the annealed CdS nanorods was well crystallized, while that of the unannealed nanorods was amorphous. Energy-dispersive x-ray spectrography, x-ray photoelectron spectrography and thermogravimetric analysis were used to demonstrate that the amorphous layer at the surface of the as-prepared nanorods was pure CdS. The photoluminescence spectra showed that after annealing the intensity of the band-edge emission increased several times and the surface state emission at 548 nm disappeared. The unannealed CdS nanorods had approximately linear I–V characteristics and the conductance suddenly increased about 100 times upon visible light illumination by a halogen lamp. The annealed CdS nanorods exhibited nonlinear conductance with a turn-on voltage at about 2.2 V. These properties show that CdS nanorods have potential applications in nanophotoelectric or sensing devices.

1. Introduction

Wide band gap semiconductor nanowires and nanorods have received considerable attention because of their potential applications as novel functional materials in nanodevices [1–4]. Because of the high surface-to-volume ratio, the physical properties of 1D semiconductor nanostructures are strongly correlated to the surface situation. Surface quality control and surface modification of ZnO nanorods/nanowires have become important areas for exploring their applications in nanoscale optoelectronic devices or solid-state sensors [5–7]. Recently, the photoluminescence intensity and quantum yield (QY) of CdS nanowires were greatly enhanced through surface capping with a ZnS shell [8]. However, little attention has been paid to the surface quality and its effect on the physical properties of CdS nanorods. In this paper, we report on the investigation of surface crystallization effects on the photoluminescence and electrical transport properties of CdS nanorods. Our results demonstrate that the surface of the CdS nanorods strongly affects the optical and electrical properties of the CdS nanorods.

2. Experimental details

CdS nanorods were synthesized through a simple solvothermal method, which is similar to the previous report given elsewhere [9], except that we use a different cadmium source and need a longer reaction time. In a typical synthesis, 0.256 g CdO and 0.064 g sulfur powder (molar ratio, 1:1) were put into a Teflon-lined stainless steel autoclave of 50 ml capacity which

[3] Author to whom any correspondence should be addressed.

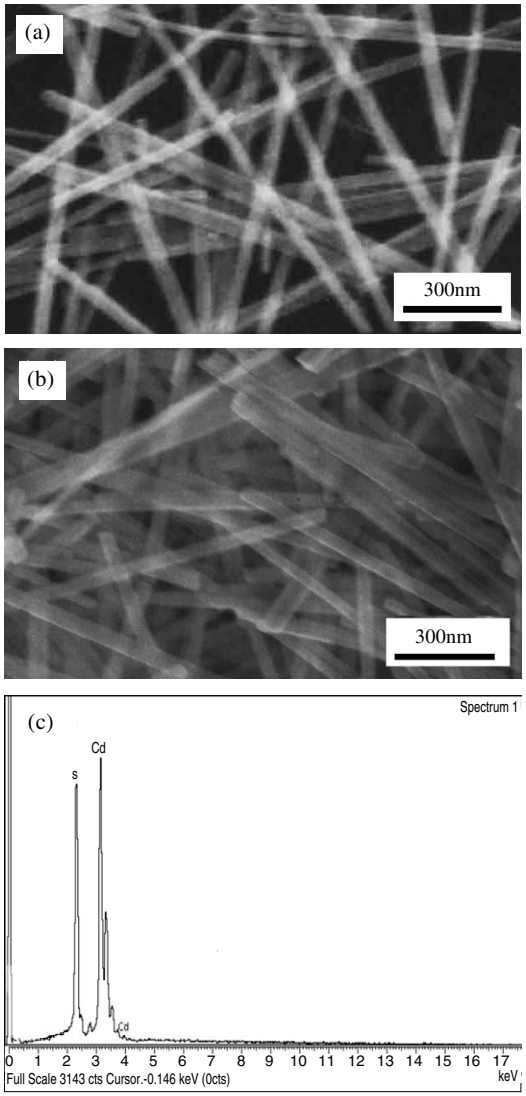

Figure 1. (a) and (b) SEM images of the unannealed and the annealed CdS nanorods, respectively. (c) The *in situ* energy-dispersive x-ray spectrum for the as-prepared nanorods.

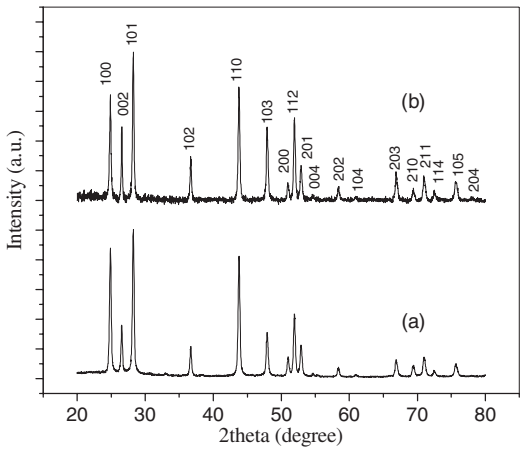

Figure 2. XRD patterns for the unannealed CdS nanorods (a), and the annealed CdS nanorods (b).

had been filled with ethylenediamine up to 80% of the total volume. The autoclave was sealed and maintained at 160 °C for 72 h and air-cooled to room temperature. The resulting white-yellow solid precipitate was washed with distilled water and absolute ethanol and dried at 60 °C in a vacuum. To obtain highly crystallized CdS nanorods, part of the as-prepared sample was further annealed at 450 °C in argon for 4 h.

X-ray diffraction (XRD) data were obtained on a Rigaku D/MAX 2400 type spectroscope (Cu Kα, wavelength: 1.541 78 Å). The morphology and structure of the samples were characterized by field-emission scanning electron microscopy (SEM, Hitachi S-5200) and high-resolution transmitted electron microscopy (HRTEM, FEG-CM 200). The x-ray photoelectron spectra were obtained on a VGESCALAB MK11 x-ray photoelectron spectrometer (XPS), using non-monochromatized Mg Kα radiation as the excitation source. Thermogravimetric analysis (TGA) experiments were performed in a thermo-gravimetric differential scanning calorimetry (TG-DSC) apparatus STA-449C (Netzsch, Germany) with the heating rate 10 °C min^{-1} in argon. Photoluminescence (PL) spectra were taken on a PTI-C-700 fluorescence spectrometer with a 325 nm He–Cd laser. The PL quantum yield (QY) of the nanorods was obtained by a reference PL technique (in ethanol), with coumarin 6 (QY = 0.78) as the reference fluorophore at 505 nm emission [10]. The PL lifetime decay profiles were measured through the following setup. Laser pulses at 793 nm (∼120 fs, 0.7 mJ, 1 kHz) were produced with a regenerative amplifier (Spitfire, Spectra Physics), which was seeded by a mode-locked Ti–sapphire laser (Tsunami, Spectra Physics). These pulses were frequency-doubled in a BaB_2O_4 (BBO) crystal to generate the second harmonic line at 397 nm, which then passed through another BBO crystal to generate a mixing signal at 266 nm. This was used as the excitation pulse with an excitation intensity ∼0.2 μJ cm^{-2}. The fluorescence was focused into a monochromator and detected using a photon counting streak camera (Hamamatsu C2909). The time resolution is 30 ps and the spectral resolution of monochromator with 150 grooves mm^{-1} grating is 0.2 nm. The electronic transport properties were conducted in a four-probe system with a semiconductor parameter analyser (Keithley Company, 4200-SCS) at room temperature in a UHV (5×10^{-8} Pa) chamber. A scanning electron microscope (SEM) was attached to this system to monitor the operations. During the measurements, two tungsten probes were directly pressing on the ends of a single CdS nanowire, which was pre-deposited on a silicon substrate with a 500 nm thick thermally grown SiO_2 layer.

3. Results and discussion

The SEM images of the as-prepared nanorods before and after annealing are shown in figures 1(a) and (b), respectively. The diameters of the nanorods in both samples are in the range of 35–45 nm, and the lengths of the nanorods are all about 2–6 μm, so the annealing process brought no apparent variety to the sizes of the nanorods. Figure 1(c) shows the *in situ* energy-dispersive x-ray spectrum for the as-prepared nanorods, which shows that only Cd and S atoms exist in the sample and the atomic percentage is 50.9 and 49.1 for Cd and S, indicating the

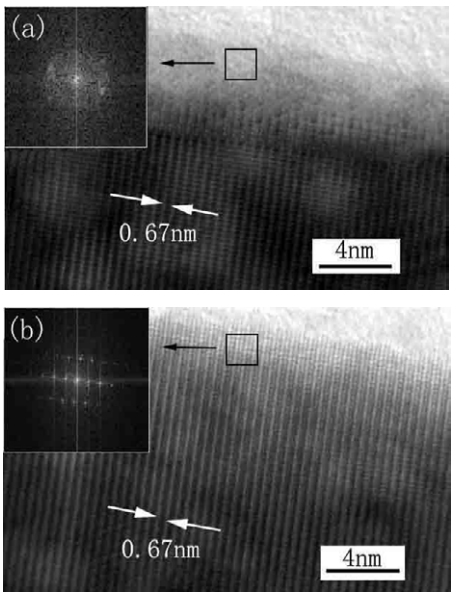

Figure 3. (a) and (b) HRTEM images of the unannealed and the annealed CdS nanorods, respectively; the images inset in the upper-left of (a) and (b) are the two-dimensional Fourier transforms from the corresponding areas indicated by rectangles.

stoichiometric composition of CdS. The energy-dispersive x-ray spectrum for the annealed nanorods is similar to that of the as-prepared one. The XRD patterns of the samples before and after annealing are shown in figures 2(a) and (b), respectively. All peaks in figures 2(a) and (b) can be indexed as those from hexagonal wurtzite CdS with lattice constants of $a = 4.141$ and $c = 6.720$ Å (JCPDS card, 41-1049). After annealing at 450 °C with the protection of argon, the morphology, the composition, and the phase of the CdS nanorods remain the same.

The nanorods were further characterized by high-resolution transmission electron microscopy (HRTEM). The HRTEM images of two representative CdS nanorods before and after annealing are shown in figures 3(a) and (b), respectively. The cores of the unannealed CdS nanorods are single crystalline, while there are an amorphous layer (∼3 nm) at their surfaces, as shown in figure 3(a). However, both the core and the surface of the annealed nanorods are perfectly single crystalline, as shown in figure 3(b). The measured interplanar distances are in agreement with the typical hexagonal wurtzite CdS(002) fringe (0.67 nm), which means that the growth direction of the nanorods is [001]. The crystallization phases at the surface of the nanorods were further displayed by two-dimensional Fourier transformations of their corresponding high-resolution images, as given in the top left insets of figures 3(a) and (b). The Fourier transformation results proved that the surfaces of CdS nanorods, before and after annealing, are amorphous and crystalline, respectively.

To further demonstrate that the amorphous layer at the surface of the as-prepared nanorods is pure CdS, without contamination, we carried out XPS and TGA examinations. Figure 4(a) shows the XPS spectrum of the as-prepared nanorods, which shows only peaks for cadmium and sulfur elements, and the ratio Cd/S is estimated to be about

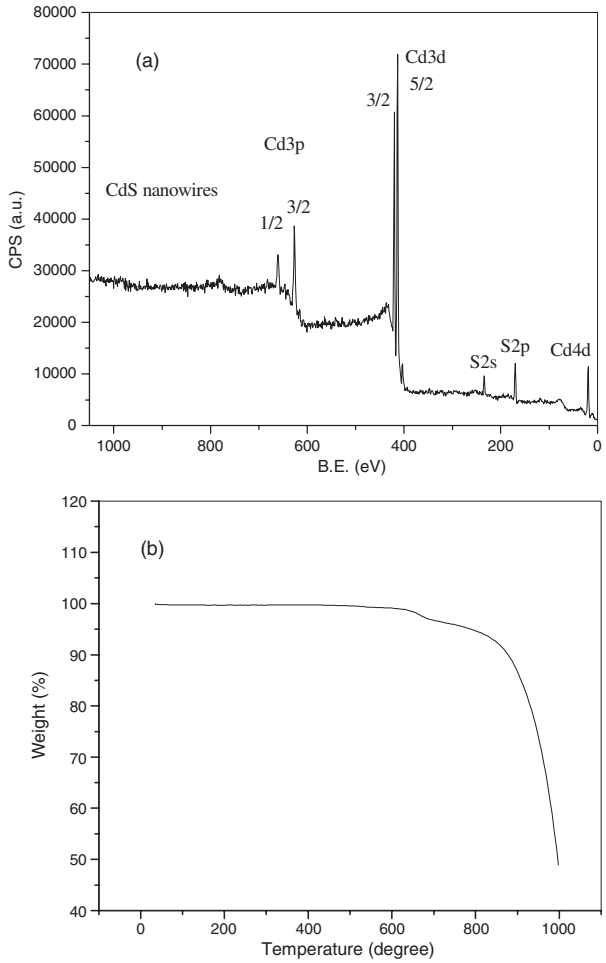

Figure 4. (a) The XPS spectrum and (b) the TGA curve of the as-prepared nanorods.

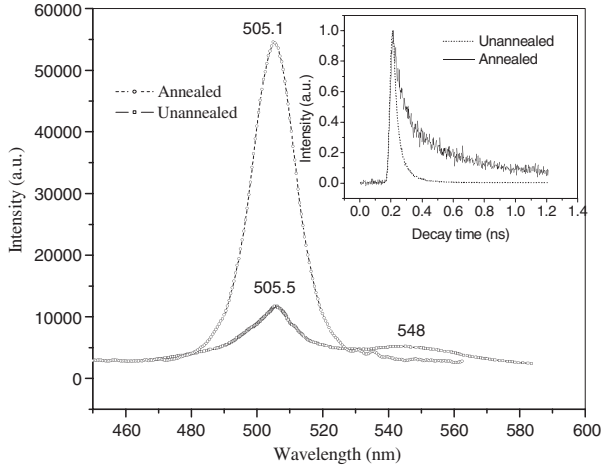

Figure 5. PL spectra for the unannealed CdS nanorods (solid line) and the annealed CdS nanorods (dotted line). Inset: the lifetime decay profiles of the unannealed nanorods (dotted line) and the annealed nanorods (solid line).

1.01:1. Since XPS only reflects the surface information of the examined sample, the above result indicates that the amorphous layer of the sample is composed of CdS. Figure 4(b)

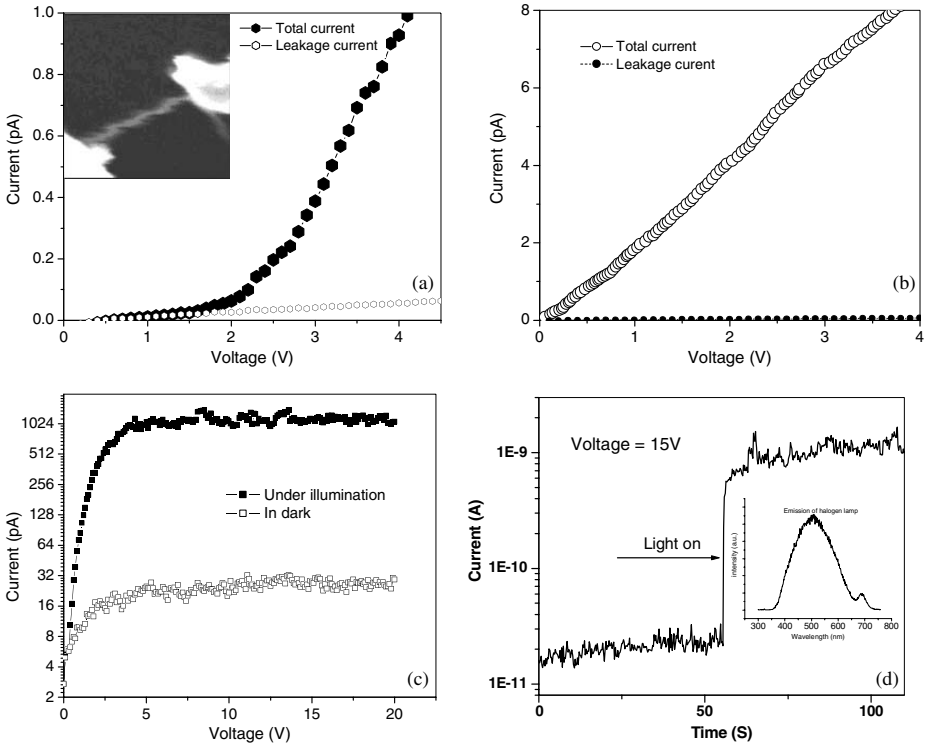

Figure 6. (a) The current–voltage (I–V) curve of one representative annealed CdS nanowire; the inset shows the SEM image of the CdS nanowire with two tungsten probes attached to it. (b) The I–V curve of one representative unannealed CdS nanorods. (c) The I–V curves of one individual unannealed CdS nanowire before and after visible light illumination with a halogen lamp. (d) The conductance increase under visible light illumination with a very large jumping rate. The inset of figure 4(d) is the emission spectrum of the halogen l.

is the TGA curve of the as-prepared nanorods in argon, which shows no apparent weight loss below ∼600 °C. The weight loss above 600 °C comes from the decomposition and sublimation of CdS. This result indicates that there are no organic residues on the surface of the nanorods and simultaneously shows that the CdS nanorods are stable below 600 °C in argon.

The PL spectra of the annealed sample and the corresponding unannealed sample are shown in figure 5. Both samples show a sharp emission band at around 505 nm, which is attributed to the typical band–band transitions of CdS crystal since the spectral position is very near the band gap of CdS (2.47 eV) at room temperature [11, 12]. The band-edge emission of the annealed nanorods is several times stronger than that of the unannealed sample, and the quantum yield is increased from ∼0.2% to ∼1.5% through the annealing. The unannealed sample has another broad emission band around 548 nm, arising from the electron–hole recombination at the surface of the particle [13, 14], while there is no distinct surface-trap related emission in the annealed sample. Xu *et al* [15] also examined the PL properties of CdS nanowires and observed a broad emission band centred at 696 nm, which is associated with sulfur vacancies in the CdS crystals [14]. The absence of the sulfur vacancy-related emission in the PL spectra (figure 5) indicates that our prepared CdS nanorods are highly crystallized in the interior. The lifetime decay profiles of the samples are shown in the inset of figure 5. Both decay profiles can be fitted quite well into a biexponential function. The two time constants of the fitted curve for the decay profile of the unannealed nanorods are 20 and 71 ps, and those of the fitted curve for the decay profile of the annealed nanorods are 67 and 548 ps. Compared with that of the unannealed sample, the PL lifetime of the annealed one is significantly longer, which further demonstrates the high exciton stability relative to the high crystallization of the annealed nanorods.

The conductivities of individual CdS nanorods measured by the four-probe system are shown in figure 6. Figure 6(a) is the current–voltage (I–V) curve of one representative annealed CdS nanowire with a turn-on voltage of about 2.2 V, which directly reveals a typical semiconducting conductance. The inset image in figure 6(a) shows the SEM image of a CdS nanowire with two tungsten probes attached to it. Figure 6(b) is the I–V curve of one representative unannealed nanowire. This nanowire shows linear I–V characteristics. From figure 6 we can tell that the contacts for both representative nanorods are ohmic contacts, since both I–V curves are linear in the range of 0–1 V. Therefore, the difference between figures 6(a) and (b) should originate from the intrinsic properties of the two kinds of nanorod.

Usually, CdS nanorods are synthesized with the assistance of a surfactant or a polymer template [16–20], which would contaminate the surface of nanorods. In our method, this contamination does not occur because we did not use a surfactant or a polymer template. In addition, we can also see from the HRTEM that the core of the unannealed nanorods is highly crystallized, so the annealing process should have a minor effect on the core. The differences of PL spectra and electrical conduction between the unannealed and the

annealed nanorods should mainly be attributed to the different electronic states due to the varied crystallization at the surface region of these two kinds of nanorods. Since amorphous material has quasi-continuum electronic states with a definite density of states [21], the amorphous layer at the surface of the unannealed CdS nanorods produces in-gap states with a countable density of states. The in-gap states effectively dissipate the band-edge emission energy through surface-trap related emission (figure 5) and/or nonradiative relaxation. At the same time, these quasi-continuum in-gap states increase the carrier density near the Fermi level at room temperature and lead to the linear conductance. The great increase of PL decay time in the annealed CdS nanorods compared to the unannealed ones gives further evidence that the annealed nanorods have fewer trapping states, reflecting high crystallization near their surface area. The unannealed nanorods show fast trapping of carriers with much shorter lifetime, indicating the existence of in-gap states. Moreover, these in-gap states do not come from surface contamination, so the surface amorphous structure should be the dominant origin. Therefore the difference of the PL and electrical transport properties of the CdS nanorods before and after annealing can reasonably be attributed to their different surface crystallization.

In addition, we analysed the photoelectronic response of the as-prepared unannealed nanorods with visible light illumination by a 15 W commercial halogen lamp (see the inset of figure 6(d) for the emission spectrum of this lamp). Figure 6(c) shows the I–V curves of an individual unannealed nanowire before and after illumination (the sample is 10 cm from the halogen lamp). The conductance increased about 100 times upon illumination with a very fast jumping rate (figure 6(d)). The rise in conductance is due to the generation of photocurrent, which directly increases the density of conducting carriers in the nanowire. The high sensitivity of the CdS nanorods to visible light illumination indicates potential applications in photoelectric and sensing devices.

4. Conclusion

Two kinds of CdS nanorods were obtained by a chemical process. The optical and electrical investigations indicated that the thin amorphous layer at the surface of CdS nanorods quenched most of the band-edge emission and induced the conduction from nonlinear type to linear type, in contrast to the crystalline surface of nanorods. These results indicate that the quality of surface crystallization has important influences on the optical and electrical properties of CdS nanorods. The as-prepared unannealed CdS nanorods show good optoelectronic response for the fabrication of photoelectric and sensing devices.

Acknowledgments

The authors are grateful for the financial support of NSFC of China (Term No 20173073), National 973 Project, Nano and Bio-device Key Project of CAS, and 985 fund of Hunan University.

References

[1] Wong E W, Sheehan P E and Lieber C M 1997 *Science* **277** 1971
[2] Hu J, Odom T W and Lieber C M 1999 *Acc. Chem. Res.* **32** 435
[3] Duan X F, Huang Y, Agarwal R and Lieber C M 2003 *Nature* **42** 241
[4] Gray G R 1995 *Semiconductor Laser: Past, Present, and Future* (New York: American Institute of Physics)
[5] Wan Q, Li Q H, Chen Y J, Wang T H, He X L, Li J P and Lin C L 2004 *Appl. Phys. Lett.* **84** 3654
[6] Heo Y W, Tien L C, Norton D P, Kang B S, Ren F, Gila B P and Pearton S J 2004 *Appl. Phys. Lett.* **85** 2002
[7] Li Q H, Wan Q, Liang Y X and Wang T H 2004 *Appl. Phys. Lett.* **84** 4556
[8] Hsu Y J and Lu S Y 2004 *Chem. Commun.* **18** 2102
[9] Li Y D, Liao H W, Ding Y, Qian Y T, Yang L and Zhou G E 1998 *Chem. Mater.* **10** 2301
[10] Reynolds G A and Drexhage K H 1975 *Opt. Commun.* **13** 1975
[11] Lu S Y, Wu M L and Chen H L 2003 *J. Appl. Phys.* **93** 5789
[12] Pan A L, Ma J G, Yan X Z and Zou B S 2004 *J. Phys.: Condens. Mater.* **16** 3229
[13] Wang Y and Herron N J 1988 *J. Phys. Chem.* **92** 4988
[14] Kuczynski J and Thomas J K 1985 *J. Phys. Chem.* **89** 2720
[15] Xu D, Liu Z, Liang J and Qian Y 2005 *J. Phys. Chem.* B **109** 14344
[16] Zhan J, Yang X, Wang D, Li S, Xie Y, Xia Y and Qian Y 2000 *Adv. Mater.* **12** 1348
[17] Zhan J H, Yang X G, Wang D W, Xie Y and Qian Y T 2000 *J. Cryst. Growth.* **220** 231
[18] Jun Y, Lee S, Kang N and Cheon J 2001 *J. Am. Chem. Soc.* **123** 5150
[19] Chu Y C, Wang C C and Chen C Y 2005 *Nanotechnology* **16** 58
[20] Lu X F, Gao H, Chen J Y, Chao D M, Zhang W J and Wei Y 2005 *Nanotechnology* **16** 113
[21] Brodsky M H 1997 *Amorphous Semiconductors* (New York: Springer)